Optical properties of $Al_xGa_{1-x}As$ alloys

Sadao Adachi
Department of Electronic Engineering, Faculty of Engineering, Gunma University, Kiryu-shi, Gunma 376, Japan
(Received 13 June 1988; revised manuscript received 9 August 1988)

A method is described for calculation of the real (ϵ_1) and imaginary (ϵ_2) parts of the dielectric function of semiconductors at energies below and above the lowest direct band edge, in which the model is based on the Kramers-Kronig transformation and strongly connected with the electronic energy-band structure of the medium. The method reveals distinct structures at energies of the E_0, $E_0+\Delta_0$, E_1 ($E_1+\Delta_1$), and E_2 critical points (CP's). The indirect-gap transitions also take an important part in the spectral dependence of ϵ_2. Analyses are presented for $Al_xGa_{1-x}As$ alloys, and results are in satisfactory agreement with the experimental information over the entire range of photon energies (0–6.0 eV). The compositional dependence of the optical-transition strength at energies of each CP and indirect gap is also given and discussed.

I. INTRODUCTION

The alloy system $Al_xGa_{1-x}As/GaAs$ is potentially of great importance for many high-speed electronic and optoelectronic devices, because the lattice parameter difference between GaAs and $Al_xGa_{1-x}As$ ($0\leq x\leq 1.0$) is very small (less than 0.15% at 300 K), which promises an insignificant concentration of undesirable interface states.

Investigation of the dielectric behaviors in solids is an old topic which arises in strong connection with the fundamental optical properties of the solids.[1] Knowledge of the refractive indices and absorption coefficients of semiconductors forms an important part especially in the design of heterostructure lasers as well as other waveguiding devices with the use of these materials.[2]

Spectroscopic ellipsometry is an excellent technique to investigate the optical response of semiconductors.[3–14] Recently, Aspnes *et al.*[15] have studied optical properties of $Al_xGa_{1-x}As$ alloys of target compositions $x=0.0-0.80$ in steps of 0.10 by spectroscopic ellipsometry. They reported room-temperature pseudodielectric function data and related optical constants of $Al_xGa_{1-x}As$ alloys for energies E from 1.5 to 6.0 eV. Garriga *et al.*[16] also presented the pseudodielectric function data of AlAs, a binary endpoint of $Al_xGa_{1-x}As$ alloys, for energies between 1.7 and 5.6 eV determined by spectroscopic ellipsometry. However, these spectral-dependence data have one disadvantage with respect to theoretical modeling:[15] They are not expressed as continuous analytic functions of the electronic energy gaps and also of the alloy composition x.

In this paper, we present a method for calculation of the spectral dependence of the dielectric constants, $\epsilon_1(\omega)$ and $\epsilon_2(\omega)$, of $Al_xGa_{1-x}As$ alloys based on a simplified model of the band structure of the materials. This calculation covers the optical response of semiconductors in the entire range of photon energies. In Sec. II, we describe the details of our model which includes the E_0, $E_0+\Delta_0$, E_1, and E_2 gaps as the main dispersion mechanisms. The effects of indirect-gap transitions which will take an important part in the analysis of the ϵ_2 spectrum are also discussed. In Sec. III, we show the fits with our model to the experimental data of $Al_xGa_{1-x}As$ alloys reported by Aspnes *et al.*[15] An excellent agreement between our calculation and experimental data will be achieved in the entire range of photon energies. The compositional dependence of the strength parameter at energies of each gap is also presented and discussed in Sec. III. Finally, in Sec. IV, the conclusions obtained in this study are summarized briefly.

II. THEORETICAL EXPRESSION

The dielectric function, $\epsilon(\omega)=\epsilon_1(\omega)+i\epsilon_2(\omega)$, is known to describe the optical response of the medium at all photon energies $E=\hbar\omega$.[1] Real and imaginary parts of this dielectric function are connected by the Kramers-Kronig relations[1,17]

$$\epsilon_2(\omega)=-\frac{2}{\pi}\int_0^\infty \frac{\epsilon_1(\omega')}{(\omega')^2-\omega^2}d\omega' , \tag{1a}$$

$$\epsilon_1(\omega)-1=\frac{2}{\pi}\int_0^\infty \frac{\omega'\epsilon_2(\omega')}{(\omega')^2-\omega^2}d\omega' . \tag{1b}$$

The dielectric function is strongly connected with the electronic energy-band structures of the material.[1,18] The optical joint density of states becomes large for electronic transitions in the neighborhood of critical points (CP's). In the following, we present the model dielectric functions for the CP's of various transition energies (E_0, $E_0+\Delta_0$, E_1, and E_2). The effects of indirect-gap transitions which will take an important part in the analysis of the ϵ_2 spectrum are also discussed briefly.

A. E_0 and $E_0+\Delta_0$ transitions

The lowest direct gaps, E_0 and $E_0+\Delta_0$, are of the three-dimensional (3D) M_0-type CP's. Assuming the bands are parabolic, we obtain the contribution of these gaps to $\epsilon_2(\omega)$ and $\epsilon_1(\omega)$ (Ref. 17):

$$\epsilon_2(\omega)=[A/(\hbar\omega)^2][(\hbar\omega-E_0)^{0.5}H(\chi_0-1)+\tfrac{1}{2}(\hbar\omega-E_0-\Delta_0)^{0.5}H(\chi_{so}-1)] , \quad (2)$$

$$\epsilon_1(\omega)=AE_0^{-1.5}\{f(\chi_0)+\tfrac{1}{2}[E_0/(E_0+\Delta_0)]^{1.5}f(\chi_{so})\} , \quad (3)$$

with

$$A=\tfrac{4}{3}(\tfrac{3}{2}m^*)^{1.5}P^2 , \quad (4)$$

$$f(\chi_0)=\chi_0^{-2}[2-(1+\chi_0)^{0.5}-(1-\chi_0)^{0.5}H(1-\chi_0)] , \quad (5a)$$

$$f(\chi_{so})=\chi_{so}^{-2}[2-(1+\chi_{so})^{0.5}-(1-\chi_{so})^{0.5}H(1-\chi_{so})] , \quad (5b)$$

$$\chi_0=\hbar\omega/E_0 , \quad (6a)$$

$$\chi_{so}=\hbar\omega/(E_0+\Delta_0) , \quad (6b)$$

and

$$H(y)=\begin{cases}1 & \text{for } y\geq 0\\ 0 & \text{for } y<0 .\end{cases} \quad (7)$$

In Eq. (4), m^* is the combined density-of-states mass and P^2 is the squares momentum matrix element.

B. E_1 transitions

Band-structure calculations and some experimental work indicated[19] that the E_1 (and $E_1+\Delta_1$) transitions take place along the $\langle 111\rangle$ directions (Λ) or at L points in the Brillouin zone. These critical points are of the M_1 type. The contribution to ϵ_2 of this type is[17]

$$\epsilon_2(\omega)=\begin{cases}\pi\chi_1^{-2}[B_1-B_{11}(E_1-\hbar\omega)^{0.5}] & (\hbar\omega<E_1)\\ \pi B_1\chi_1^{-2} & (\hbar\omega\geq E_1) ,\end{cases} \quad (8)$$

with

$$\chi_1=\hbar\omega/E_1 , \quad (9)$$

where B's are the strength parameters. The longitudinal effective mass, however, is much larger than its transverse counterparts and one can treat these CP's as two-dimensional (2D) minima. The contribution to $\epsilon_2(\omega)$ and $\epsilon_1(\omega)$ of this type of 2D minima is given by

$$\epsilon_2(\omega)=\pi B_1\chi_1^{-2}H(\chi_1-1) , \quad (10)$$

$$\epsilon_1(\omega)=-B_1\chi_1^{-2}\ln(1-\chi_1^2) , \quad (11)$$

where H is a function defined by Eq. (7).

C. E_2 transitions

The more pronounced structure found in the higher-energy region than E_1 is usually labeled E_2. The nature of the E_2 transitions is more complicated, since it does not correspond to a single, well-defined CP. Because of this fact, we shall characterize the E_2 structure as that of a damped harmonic oscillator:

$$\epsilon_2(\omega)=C\chi_2\gamma/[(1-\chi_2^2)^2+\chi_2^2\gamma^2] , \quad (12)$$

$$\epsilon_1(\omega)=C(1-\chi_2^2)/[(1-\chi_2^2)^2+\chi_2^2\gamma^2] , \quad (13)$$

with

$$\chi_2=\hbar\omega/E_2 , \quad (14)$$

where C is the strength parameter and γ is the damping factor.

D. Indirect-gap transitions

The transition mechanism at the indirect gap, E_g^{ID}, is expressed by a second-order process in the perturbation. With the use of the result of second-order time-dependent perturbation calculation, we can write the contribution of the indirect optical transitions to $\epsilon_2(\omega)$ as

$$\epsilon_2(\omega)=\frac{D}{(\hbar\omega)^2}(\hbar\omega-E_g^{ID}+\hbar\omega_q)^2H(1-\chi_g) , \quad (15)$$

with

$$\chi_g=(E_g^{ID}-\hbar\omega_q)/\hbar\omega , \quad (16)$$

where D is the indirect-transition strength parameter, and $\hbar\omega_q$ is the phonon energy taking part in the indirect transitions. In Eq. (15), only the phonon absorption process is taken into account. The phonon emission process remains possible, however, the only difference from the above case is the sign of the phonon energy.

The parabolic bands extending to infinite energies implied by Eq. (15) should be nonphysical. We thus modify the model by taking into account a cutoff at the energy E_c. This modification provides

$$\epsilon_2(\omega)=\frac{D}{(\hbar\omega)^2}(\hbar\omega-E_g^{ID}+\hbar\omega_q)^2H(1-\chi_g)H(1-\chi_c) , \quad (17)$$

with

$$\chi_c=\hbar\omega/E_c . \quad (18)$$

Here, the cutoff energy is assumed to be the same value as E_1 (i.e., $E_c=E_1$).

Unfortunately, there has been no expression for the contribution to $\epsilon_1(\omega)$ of the indirect transitions. Analytical expressions for this contribution from the Kramers-Kronig transformation are also not yet available. We thus take into account the contribution of the indirect transitions only to $\epsilon_2(\omega)$ but not to $\epsilon_1(\omega)$.

III. RESULTS AND DISCUSSION

A. A comparison of our model to experimental spectra

The model given in Sec. II can be used to fit the experimental dispersion of ϵ_2 and ϵ_1 over most of the spectral range (0–6.0 eV). The parameters, such as A, B_1, and C can be commonly used as adjustable constants for calculations of both ϵ_2 and ϵ_1. The experimental data of ϵ_1 in the transparent region are, however, usually somewhat larger or smaller than our model [i.e., the sum of Eqs. (3), (11), and (13)]. In order to improve a fit, therefore, we shall consider an additional term, $\epsilon_{1\infty}$, to ϵ_1. This term is

assumed to be nondispersive (i.e., constant) and may arise from the indirect-gap and other higher-gap transitions (E_0', $E_0'+\Delta_0'$, E_1', $E_1'+\Delta_1'$, etc.).

The fits with our model to the experimental ϵ_2 and ϵ_1 of $Al_xGa_{1-x}As$ ($x=0.315$) (Ref. 15) are shown in Figs. 1 and 2, respectively. The $Al_{0.315}Ga_{0.685}As$ is a direct-band-gap semiconductor. The lowest direct gaps E_0 ($\Gamma_8^v \rightarrow \Gamma_6^c$) and $E_0+\Delta_0$ ($\Gamma_7^v \rightarrow \Gamma_6^c$) are, respectively, 1.83 and 2.15 eV at room temperature.[20] The E_1 and $E_1+\Delta_1$ transitions occur at 3.13 and 3.35 eV, respectively.[15,20] The contribution to ϵ_2 of the $E_1+\Delta_1$ transitions (3D CP) can be given in a similar form as Eq. (8), i.e.,

$$\epsilon_2(\omega)=\begin{cases}\pi\chi_{1s}^{-2}[B_2-B_{21}(E_1+\Delta_1-\hbar\omega)^{0.5}] & (\hbar\omega<E_1+\Delta_1)\\ \pi B_2\chi_{1s}^{-2} & (\hbar\omega\geq E_1+\Delta_1)\end{cases}, \tag{19}$$

with

$$\chi_{1s}=\hbar\omega/(E_1+\Delta_1)\ , \tag{20}$$

where B_2 and B_{21} are the strength parameters corresponding to the $E_1+\Delta_1$ transitions. The contributions to ϵ_2 and ϵ_1 of the $E_1+\Delta_1$ transitions with a 2D-CP treatment are also given by

$$\epsilon_2(\omega)=\pi B_2\chi_{1s}^{-2}H(\chi_{1s}-1)\ , \tag{21}$$

$$\epsilon_1(\omega)=-B_2\chi_{1s}^{-2}\ln(1-\chi_{1s}^2)\ . \tag{22}$$

The strength of the E_1 and $E_1+\Delta_1$ transitions of zinc-blende materials can be estimated with the simple expression[5-7]

$$B_1=44\frac{(E_1+\Delta_1/3)}{a_0E_1^2}\ , \tag{23a}$$

$$B_2=44\frac{(E_1+2\Delta_1/3)}{a_0(E_1+\Delta_1)^2}\ , \tag{23b}$$

where a_0 is the lattice constant in Å and E_1,Δ_1 in eV. The splitting energies Δ_1 in the $Al_xGa_{1-x}As$ alloy system are, however, rather small (≤ 0.23 eV) (Ref. 20) over the entire range of alloy composition, and can be successfully neglected here. (The E_1 transitions can take over the $E_1+\Delta_1$ gap contribution.)

The $Al_{0.315}Ga_{0.685}As$ has indirect gaps, $\Gamma_8^v \rightarrow L_6^c$ near 1.92 eV (E_g^L) and $\Gamma_8^v \rightarrow X_6^c$ near 1.94 eV (E_g^X).[21] The indirect transitions, thus, take part at above the onset of the direct-gap transitions which occurs at 1.83 eV (E_0). The structure that appeared in the region ~ 4.7 eV is labeled to be E_2.[20]

In Fig. 1, the solid line is obtained from the sum of Eqs. (2), (8), (12), and (17). The dashed line is the result of the sum of Eqs. (2), (10), and (12). The parameters of the fits are listed in Table I. As discussed in Sec. II, we are

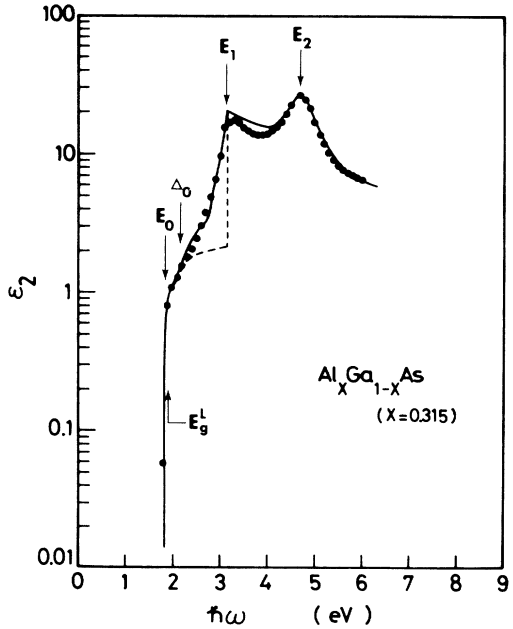

FIG. 1. ϵ_2 spectrum of $Al_{0.315}Ga_{0.685}As$ alloys. The experimental data (solid circles) are taken from Ref. 15. The solid line is obtained from the sum of Eqs. (2), (8), (12), and (17). The dashed line is taken by the sum of Eqs. (2), (10), and (12).

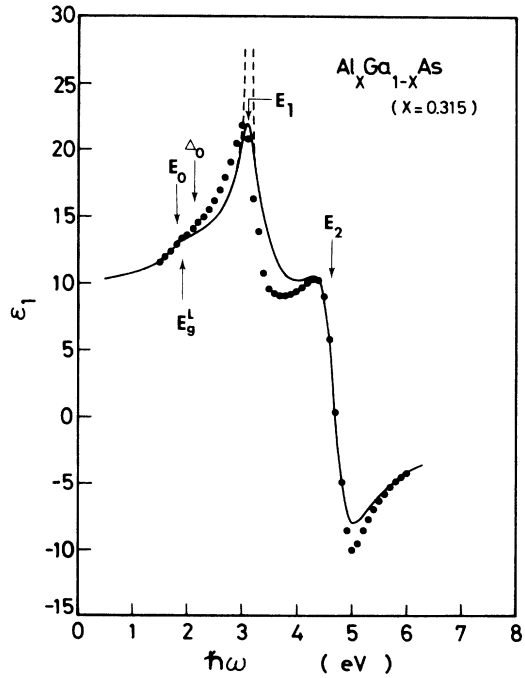

FIG. 2. ϵ_1 spectrum of $Al_{0.315}Ga_{0.685}As$ alloys. The experimental data (solid circles) are taken from Ref. 15. The solid line is obtained from the sum of Eqs. (3), (11) ($\Gamma=0.11$ eV; see text), and (13). The dashed line is taken by the sum of Eqs. (3), (11) ($\Gamma=0$ eV; see text), and (13). The nondispersive term, $\epsilon_\infty(=0.6)$ is taken into consideration in these calculations.

TABLE I. Parameters used in the calculation of $\epsilon(\omega)$ and $\epsilon_2(\omega)$.

Parameter	X								
	0.000	0.099	0.198	0.315	0.419	0.491	0.590	0.700	0.804
E_0 (eV)	1.42	1.54	1.67	1.83	1.97	2.08	2.24	2.42	2.59
$E_0+\Delta_0$ (eV)	1.77	1.88	2.00	2.15	2.30	2.40	2.55	2.73	2.90
E_1 (eV)	2.90	3.00	3.06	3.13	3.19	3.24	3.32	3.43	3.56
E_2 (eV)	4.7	4.7	4.7	4.7	4.7	4.7	4.7	4.7	4.7
E_g^{ID} (eV)	1.73[a]	1.79[a]	1.85[a]	1.92[a]	1.96[b]	1.97[b]	2.00[b]	2.03[b]	2.07[b]
A ($eV^{1.5}$)	3.45	4.21	4.58	8.80	8.96	12.55	15.40	23.20	30.63
B_1	6.37	6.37	6.37	6.05	5.73	5.73	5.41	5.41	5.09
B_{11} ($eV^{-0.5}$)	13.08	9.99	11.27	11.05	10.89	10.22	10.44	9.55	10.21
Γ (eV)	0.10	0.10	0.11	0.11	0.11	0.12	0.12	0.12	0.11
C	2.39	2.31	2.09	2.30	2.45	2.22	2.32	1.76	1.35
γ	0.146	0.129	0.127	0.135	0.138	0.127	0.131	0.103	0.080
D	24.2	21.3	19.0	16.1	13.8	10.0	9.2	8.1	7.0
$\epsilon_{1\infty}$	1.6	1.4	1.2	0.6	0.5	0.3	0.0	−0.3	−0.4

[a] E_g^L ($\Gamma_8^v \rightarrow L_6^c$ transitions).
[b] E_g^X ($\Gamma_8^v \rightarrow X_6^c$ transitions).

able to fit the E_1 CP structure with either a 2D [Eq. (10)] or 3D model [Eq. (8)]. The 3D model well explains the experimental lower-energy shoulder of this structure. The fit in the 2–3 eV region also becomes satisfactory when the indirect-gap contribution [Eq. (17)] is taken into account. The E_2 structure is seen to be well fitted by the damped harmonic oscillator [Eq. (12)].

In Fig. 2, the solid and dashed lines are obtained from the sum of Eqs. (3), (11), and (13). The nondispersive term, $\epsilon_{1\infty}$ ($=0.6$), is taken into consideration in these calculations. The theoretical ϵ_1 spectrum [Eq. (11)] exhibits a divergence at the E_1 edge. It is well known that the optical transitions are strongly affected by a damping effect, i.e., a lifetime broadening. The damping effect can be easily introduced in Eq. (11) in a phenomenological manner by replacing ω by $\omega+i(\Gamma/\hbar)$. Variation of $\epsilon_1(\omega)$ for a particular choice of the damping energy Γ is shown in Fig. 2 by the dashed ($\Gamma=0$ eV) and solid lines ($\Gamma=0.11$ eV). As seen in the figure, the damping effect can decrease the strength of the E_1 structure and lead to a fact which is coincident with experimental verification. It is also seen that a dramatic change in $\epsilon_1(\omega)$ near the E_2 edge region can be well fitted by the damped harmonic oscillator model of the E_2 structure [Eq. (13)].

A comparison of our ϵ_2 and ϵ_1 models to the experimental data of $Al_xGa_{1-x}As$ ($x=0.700$) (Ref. 15) is shown in Figs. 3 and 4, respectively. There have been several determinations of the compositional dependence of the fundamental absorption edges in $Al_xGa_{1-x}As$.[22] These studies indicate that the Γ-X crossover occurs in the compositional range of $0.4 \lesssim x \lesssim 0.5$. This region of x where the bands cross is relatively uncertain at the present time. In $Al_{0.700}Ga_{0.300}As$, an indirect-gap material, the lowest conduction minimum is located at X and the second and third set of conduction minima, respectively, lay 0.13 eV (L_6^c) and 0.39 eV (Γ_6^c) above the X minima.[21] The lowest direct gap E_0 ($E_0+\Delta_0$) of $Al_{0.700}Ga_{0.300}As$, $\Gamma_8^v \rightarrow \Gamma_6^c$ ($\Gamma_7^v \rightarrow \Gamma_6^c$), is 2.42 eV (2.73 eV),[20] and the indirect gaps E_g^X ($\Gamma_8^v \rightarrow X_6^c$) and E_g^L ($\Gamma_8^v \rightarrow L_6^c$) are, respectively, 2.03 and 2.16 eV at room temperature.[21] The indirect transitions in $Al_{0.700}Ga_{0.300}As$, thus, take part at below the onset of the direct-gap transitions which occurs at 2.42 eV. This is in contrast with the case for $Al_{0.315}Ga_{0.685}As$ in which the indirect transitions occur after the onset of the direct transitions. The E_1 and E_2 transitions occur at 3.43 and 4.7 eV, respectively.[15,20]

In Fig. 3, the solid line represents the result of the sum of Eqs. (2), (8), (12), and (17), and the dashed line corresponds to the sum of Eqs. (2), (10), and (12). The fit in the

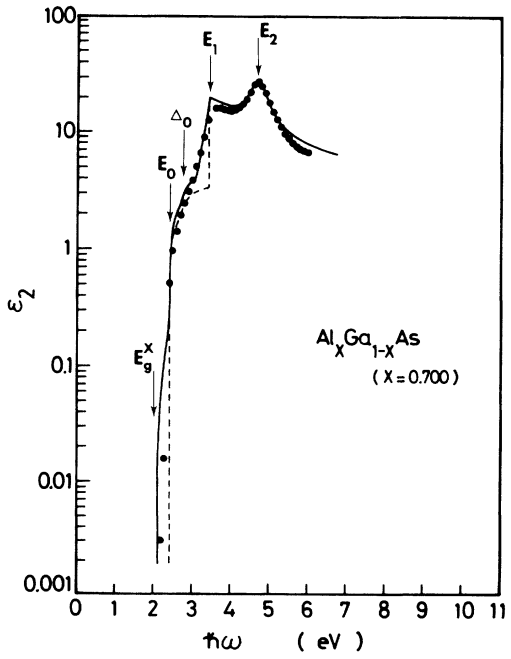

FIG. 3. ϵ_2 spectrum of $Al_{0.700}Ga_{0.300}As$ alloys. The experimental data (solid circles) are taken from Ref. 15. The solid line is obtained from the sum of Eqs. (2), (8), (12), and (17). The dashed line is taken by the sum of Eqs. (2), (10), and (12).

fundamental absorption edge region becomes quite satisfactory when the indirect-gap contribution [Eq. (17)] is taken into account. The 3D saddle-point term [Eq. (8)] also well interprets the E_1 region of the ϵ_2 spectrum. An excellent agreement can, thus, be achieved between our model (solid line) and experimental data over a wide range of the photon energies.

In Fig. 4, the dashed line represents the dependence of ϵ_1 on ω obtained from the sum of Eqs. (3), (11) ($\Gamma=0$ eV), and (13). The experimental value of ϵ_1 at the E_1 peak is 20.334.[15] As discussed before, the smaller the damping energy gives the larger the E_1 peak value. The calculation of Eq. (11) with $\Gamma=0.12$ eV agrees well with this value (solid line). Equation (13) also well interprets the peculiar line shape of the E_2 structure.

An individual contribution to ϵ_2 of the $E_0/(E_0+\Delta_0)$, E_g^{ID}, E_1, and E_2 gaps for $Al_{0.315}Ga_{0.685}As$ and $Al_{0.700}Ga_{0.300}As$ alloys is shown in Figs. 5 and 6, respectively. They are obtained from Eq. (2) for the $E_0/(E_0+\Delta_0)$ gap contribution, from Eq. (17) for the E_g^{ID} gap one, from Eq. (8) (solid line) and Eq. (10) (dashed line) for the E_1 gap one, and from Eq. (12) for the E_2 gap one.

The transitions at the M_0 edges $[E_0/(E_0+\Delta_0)]$ yield a continuous absorption obeying the well-known $\frac{1}{2}$-power law [i.e., $\propto(\hbar\omega-E_0)^{0.5}$]. The transitions at the E_g^{ID} gap provide a gradually increasing absorption spectrum characterized by a power law of $(\hbar\omega-E_g^{ID})^2$. Because of the low probability for indirect transitions, one can only expect to realize them experimentally below the direct threshold as a tail of the direct absorption edge (see Fig. 3). The steep high-energy end of the E_g^{ID} gap contribution in Figs. 5 and 6 is the result of the E_c cut-off energy modification. The E_g^{ID} transitions may also occur at energies above E_c. However, the ensuing E_1 and E_2 transitions can provide sufficient strength and, thus, take over the indirect-gap oscillators present at above E_c.

The E_1 gap is of the 3D M_1 (2D M_0) type. Hence, the lineshape of corresponding ϵ_2 spectrum should be characterized by a steep low-energy side and a broader high-energy side. This line shape is in good agreement with the experimental data.

As seen in Figs. 1–4, the E_2 structure can be well characterized by the damped harmonic oscillator model [Eqs. (12) and (13)]. This model of ϵ_2 gives a Lorentzian-like line shape (see Figs. 5 and 6), and in the limit $\gamma\rightarrow 0$ ϵ_2 spectrum exhibits a divergence at $\hbar\omega=E_2$. We can also consider the E_2 gap as the CP of 2D M_1 type. The contribution to ϵ_2 of this type is

$$\epsilon_2(\omega)=\pi\chi_2^{-2}(C_1\ln|1-\chi_2|-C_2)\ , \tag{24}$$

where C's are the strength parameters. Equation (24) exhibits a divergence at $\chi_2=1.0$ ($\hbar\omega=E_2$), and its spectrum resembles that of the damped harmonic oscillator when we take into account the damping effect in the model. Thus, the E_2 structure may be of the 2D M_1 type in good representation.

Wemple and DiDomenico[23] have proposed a semi-empirical single-effective-oscillator (SEO) model to analyze refractive-index dispersion in more than 100 widely different solids and liquids. Their model requires two parameters, E_p and E_d, where the imaginary part of the dielectric constant (ϵ_2) of the material was assumed to be a δ function at energy E_p and the strength of an effective oscillator at energy E_p was defined to be $\pi E_d/2$. In Figs.

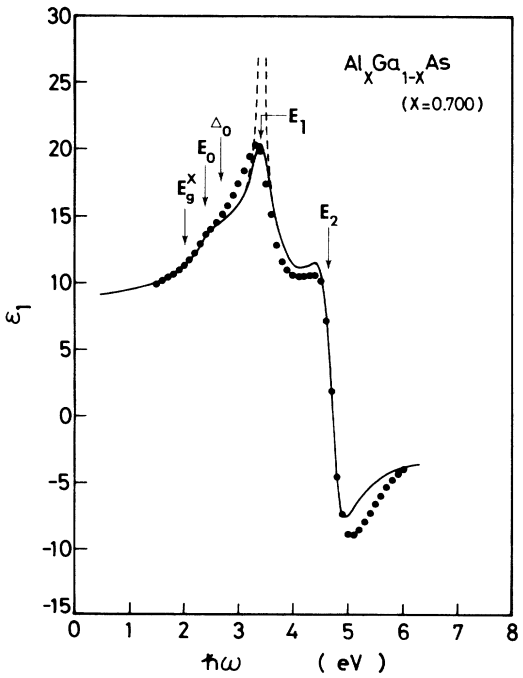

FIG. 4. ϵ_1 spectrum of $Al_{0.700}Ga_{0.300}As$ alloys. The experimental data (solid circles) are taken from Ref. 15. The solid line is obtained from the sum of Eqs. (3), (11) ($\Gamma=0.12$ eV; see text), and (13). The dashed line is taken by the sum of Eqs. (3), (11) ($\Gamma=0$ eV; see text), and (13). The nondispersive term, ϵ_∞ ($=-0.3$) is taken into consideration in these calculations.

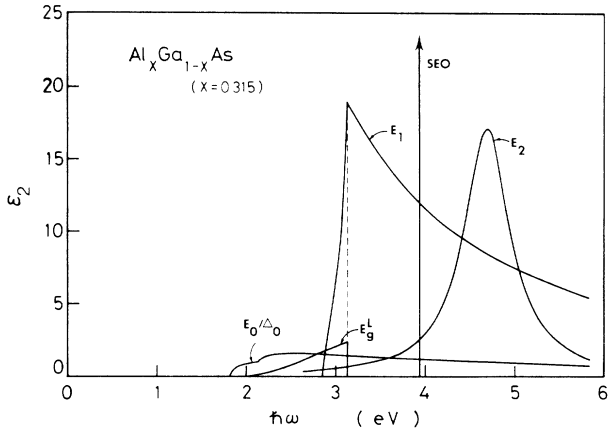

FIG. 5. Individual contribution to ϵ_2 of the $E_0/(E_0+\Delta_0)$, E_g^{ID}, E_1, and E_2 gaps for $Al_{0.315}Ga_{0.685}As$ alloys. They are obtained from Eq. (2) for the $E_0/(E_0+\Delta_0)$ gap contribution (marked by E_0/Δ_0), from Eq. (17) for the E_g^{ID} gap one, from Eq. (8) (solid line) and Eq. (10) (dashed line) for the E_1 gap one, and from Eq. (12) for the E_2 gap one. δ function (SEO) represent a single-effective-oscillator model (Ref. 23).

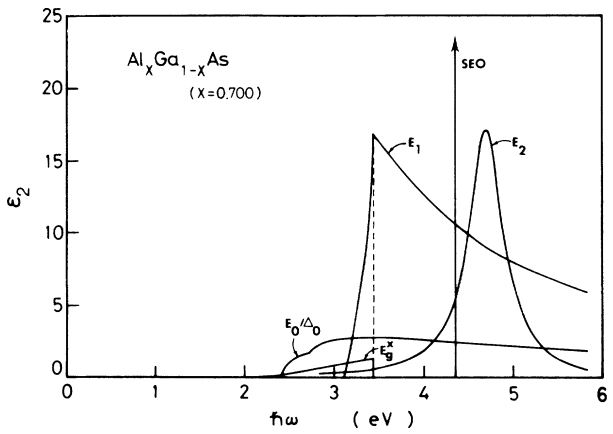

FIG. 6. As Fig. 5, but for $Al_{0.700}Ga_{0.300}As$ alloy.

5 and 6, δ functions represent the SEO model.

Matters are complicated by the lack of agreement of the data, e.g., for GaAs, with the Wemple-DiDomenico model at the direct absorption edge (E_0). Afromowitz[24] has, therefore, proposed a modified SEO model which takes into account the direct absorption edge. The spectrum proposed by Afromowitz has a form of $\epsilon_2 \propto (\hbar\omega)^4$ which is purely phenomenological and agrees with the data only on the low-energy side of the spectrum.[17]

B. Strength parameters as a function of alloy composition

The strength of the $E_0/(E_0+\Delta_0)$ transitions is represented by A [see Eq. (4)]. These transitions contribute strongly to the dispersion of $\epsilon_1(\omega)$ but not to its absolute value.[21] The numerical values of A as a function of alloy composition x for $Al_xGa_{1-x}As$, determined by fitting our model with the experimental data, are shown in Fig. 7. The plots suggest that the value of A varies almost linearly with composition x for $x \lesssim 0.5$. For $x > 0.5$, A increases abruptly with increasing x.

The lowest-direct gap E_0 varies widely by material to material for a family of the III-V compounds. In our previous paper,[25] we proceeded to find some relations between the values of A and E_0 for a number of the III-V compounds, and obtained that A increases with increasing the value of E_0. This means that the smaller E_0 gap material has smaller E_0 gap contribution (A); in other words, the smaller E_0 gap material has weaker strength of the E_0 transitions. We can recognize this general trend again, because the larger the x value is, the higher the E_0 gap energy for $Al_xGa_{1-x}As$ will be.[20]

The contribution to the dielectric susceptibility arises dominantly from the E_1 transitions. The strength of the E_1 transitions is represented by B_1 [see Eqs. (10) and (11)]. In Fig. 8, we show the variation of B_1 and Γ as a function of alloy composition x for $Al_xGa_{1-x}As$. The plots suggest that both B_1 and Γ vary relatively slowly and almost linearly with composition x.

The strength parameter B_1 can be given theoretically by[26]

$$B_1 = \frac{32\sqrt{3}}{9\omega_1}\left[\frac{a_B}{a_0}\right], \tag{25}$$

where a_B is the Bohr radius in Å, a_0 the lattice constant in Å, and ω_1 the E_1 gap energy in hartree (27.2 eV). Equation (25) predicts, for example, $B_1=5.41$ for $x=0$ and $B_1=4.41$ for $x=0.804$ at room temperature, while we found $B_1=6.4$ for $x=0$ and $B_1=5.1$ for $x=0.804$. The agreement is extremely good in view of the crudeness of the theory used. A difference between the theoretical and experimental values of B_1 has, however, been found for Ge,[5] InSb,[6] and GaP,[27] a fact which has been attribut-

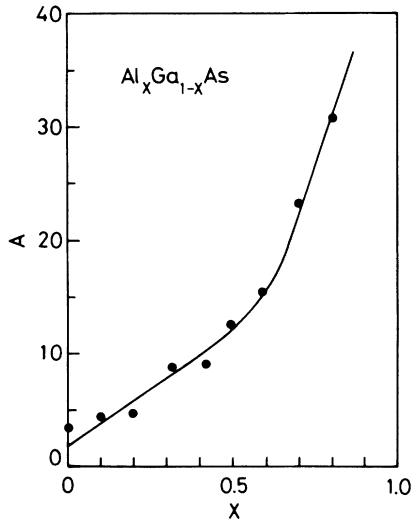

FIG. 7. The strength parameter A [$E_0/(E_0+\Delta_0)$ transitions] as a function of alloy composition x for $Al_xGa_{1-x}As$.

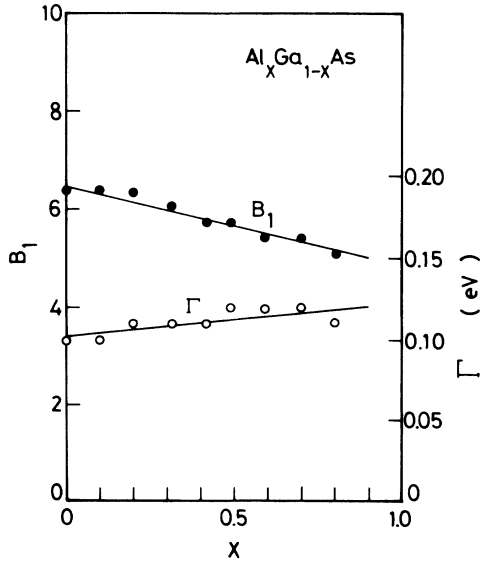

FIG. 8. The strength parameter B_1 and broadening factor Γ (E_1 transitions) as a function of alloy composition x for $Al_xGa_{1-x}As$.

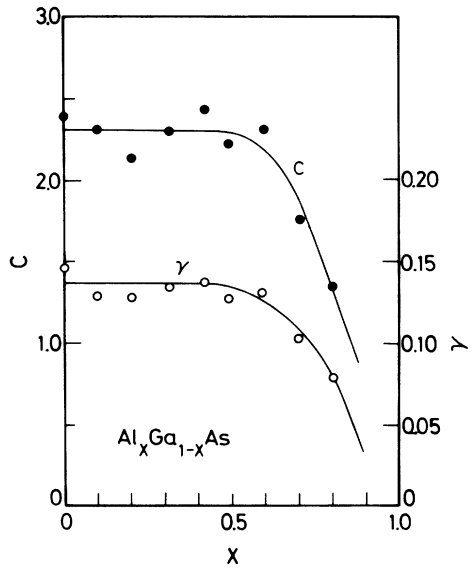

FIG. 9. The strength parameter C and broadening factor γ (E_2 transitions) as a function of alloy composition x for $Al_xGa_{1-x}As$.

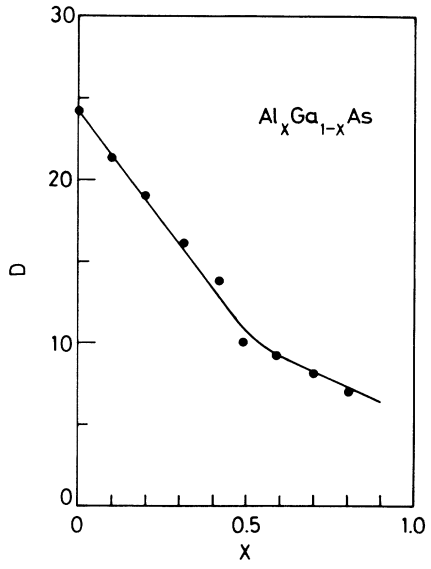

FIG. 10. The strength parameter D (indirect-gap transitions) as a function of alloy composition x for $Al_xGa_{1-x}As$.

ed to excitonic enhancement of the E_1 transitions (see also Ref. 28).

The strength of the E_2 transitions is represented by C [see Eqs. (12) and (13)]. The variation of C and γ as a function of alloy composition x for $Al_xGa_{1-x}As$ is shown in Fig. 9. Both C and γ are nearly constant up to $x \sim 0.5$, and decrease abruptly with increasing x

Information on material properties of $Al_xGa_{1-x}As$ alloys has been usually hampered by a lack of accurate experimental data on these alloys. One of the reasons of this scarcity of experimental data is the high reactivity and hygroscopicity of the $Al_xGa_{1-x}As$ alloys. The behavior of $\epsilon_1(\omega)$ at $\hbar\omega = 1.5$ eV and of the E_2 peak in $\epsilon_2(\omega)$ showed[15] that scatter in these data is less than 1% of the peak values of the spectra for $x \leq 0.5$. For $x \geq 0.6$, the peak data appeared to show systematic discrepancies indicating that chemical cleaning cannot completely remove surface overlayers on high Al content alloys. The ϵ_1 ($\hbar\omega = 1.5$ eV) quantity, on the other hand, was relatively independent of surface effects. Thus, the decrease in C and γ for samples with a higher Al content would be the result of distortion by surface degradation (i.e., oxide overlayers).

The strength of the E_g^{ID} (indirect interband) transitions can be represented by D [see Eqs. (15) and (17)]. The D is the matrix element of the combined interactions H_{ER} (electron-radiation) and H_{EL} (electron-lattice) coming from the second-order perturbation. In Fig. 10, we show the variation of D as a function of alloy composition x for $Al_xGa_{1-x}As$. The plots suggest that D varies almost linearly with x for $x < 0.5$. For $x > 0.5$, it also varies linearly with x but relatively slower.

The $Al_xGa_{1-x}As$ alloy system shows a transition between the direct and indirect structures at compositions of $x \sim 0.45$.[22] The conduction-band L-X crossover also occurs at compositions of $x \sim 0.4$:[21] the lowest conduction (satellite) band is located at L for $x < 0.4$ while it is located at X for $x > 0.4$. Such a complex conduction-band diagram may produce additional interactions between the Γ, L, and X bands in the indirect transition processes. To exactly describe the compositional dependence of D, these type of interactions must be taken into consideration. Because of the originally higher-perturbation processes of the E_g^{ID} transitions, its optical density is weaker than that of the direct-gap transitions (see Figs. 5 and 6). This may limit an accurate experimental determination of the E_g^{ID} strength. We, therefore, resignedly undertake no detailed discussion on the alloy-compositional dependence of the E_g^{ID} strength (D). However, to our knowledge, the present data is the first one informing us of the compositional dependence of the indirect optical-transition strength in alloys.

IV. CONCLUSION

We have developed a method for calculation of the real (ϵ_1) and imaginary (ϵ_2) parts of the dielectric function of semiconductors at energies below and above the lowest-direct band edge. The model is based on the Kramers-Kronig transformation and takes into account the effects of optical transitions at the E_0, $E_0+\Delta_0$, E_1, and E_2 critical points (CP's) and indirect gaps. Analyses are presented for $Al_xGa_{1-x}As$ alloys, and the results are in satisfactory agreement with the experimental data over the entire range of photon energies (0–6.0 eV). Line-shape behaviors of ϵ_1 and ϵ_2 suggest that the E_0 (E_0/Δ_0), E_1, and E_2 CP's are of the three-dimensional M_0, two-dimensional M_0 (or three-dimensional M_1), and a broadened two-dimensional M_1 type, respectively. The compositional dependence of the optical-transition strength at energies of each CP and indirect gap is also obtained and discussed. Dielectric-connected optical

constants, such as the refractive indices and the absorption coefficients, are easy to obtain from the present study in the form of practical functions. Since these expressions are purely analytical functions of the electronic energy-band parameters, the model would also be applicable to the analysis of some perturbation-induced effects of the optical constants (e.g., the pressure and temperature dependence of the refractive indices).

[1]J. Friedel, G. Harbeke, F. Abeles, B. O. Seraphin, J. Tauc, V. M. Granovich, J. G. Mavroides, M. Balkanski, H. Pick, W. E. Spicer, J. Ducuing, and C. Flytzanis, in *Optical Properties of Solids,* edited by F. Abelés (North-Holland, Amsterdam, 1972).

[2]H. C. Casey, Jr., and M. B. Panish, *Heterostructure Lasers* (Academic, New York, 1978), Pts. A and B.

[3]S. M. Kelso, D. E. Aspnes, M. A. Pollack, and R. E. Nahory, Phys. Rev. B **26**, 6669 (1982).

[4]D. E. Aspnes and A. A. Studna, Phys. Rev. B **27**, 985 (1983).

[5]L. Viña, S. Logothetidis, and M. Cardona, Phys. Rev. B **30**, 1979 (1984).

[6]S. Logothetidis, L. Viña, and M. Cardona, Phys. Rev. B **31**, 947 (1985).

[7]L. Viña, H. Höchst, and M. Cardona, Phys. Rev. B **31**, 958 (1985).

[8]M. Ermän, J. P. Andre, and J. LeBris, J. Appl. Phys. **59**, 2019 (1986).

[9]S. Logothetidis, M. Cardona, P. Lautenschlager, and M. Garriga, Phys. Rev. B **34**, 2458 (1986).

[10]P. G. Snyder, M. C. Rost, G. H. Bu-Abbud, J. A. Woollam, and S. A. Alterrovitz, J. Appl. Phys. **60**, 3293 (1986).

[11]B. Drevillon, E. Bertran, P. Alnot, J. Olivier, and M. Razeghi, J. Appl. Phys. **60**, 3512 (1986).

[12]P. Lautenschlager, M. Garriga, and M. Cardona, Phys. Rev. B **36**, 4813 (1987).

[13]P. Lautenschlager, M. Garriga, L. Viña, and M. Cardona, Phys. Rev. B **36**, 4821 (1987).

[14]S. Logothetidis and H. M. Polatoglou, Phys. Rev. B **36**, 7491 (1987).

[15]D. E. Aspnes, S. M. Kelso, R. A. Logan, and R. Bhat, J. Appl. Phys. **60**, 754 (1986).

[16]M. Garriga, P. Lautenschlager, M. Cardona, and K. Ploog, Solid State Commun. **61**, 157 (1987).

[17]S. Adachi, Phys. Rev. B **35**, 7454 (1987).

[18]M. Alouani, L. Brey, and N. E. Christensen, Phys. Rev. B **37**, 1167 (1988).

[19]S. Logothetidis, L. Viña, and M. Cardona, Phys. Rev. B **31**, 947 (1985), and references therein.

[20]S. Adachi, J. Appl. Phys. **58**, R1 (1985).

[21]S. Adachi, J. Appl. Phys. **61**, 4869 (1987).

[22]S. Adachi, J. Appl. Phys. **58**, R1 (1985), and references therein.

[23]S. H. Wemple and M. DiDomenico, Jr., Phys. Rev. B **3**, 1338 (1971).

[24]M. A. Afromowitz, Solid State Commun. **15**, 59 (1974).

[25]S. Adachi, J. Appl. Phys. **53**, 5863 (1982).

[26]M. Cardona, in *Atomic Structure and Properties of Solids,* edited by E. Burstein (Academic, New York, 1972), p. 514.

[27]K. Strössner, S. Ves, and M. Cardona, Phys. Rev. B **32**, 6614 (1985).

[28]N. Meskini, W. Hanke, H. J. Mattausch, M. Balkanski, and M. Zouaghi, J. Phys. (Paris) **45**, 1707 (1984).